

# A Targetable Fluorescent Sensor Reveals That Copper-Deficient *SCO1* and *SCO2* Patient Cells Prioritize Mitochondrial Copper Homeostasis

Sheel C. Dodani,<sup>†</sup> Scot C. Leary,<sup>§</sup> Paul A. Cobine,<sup>||</sup> Dennis R. Winge,<sup>⊥</sup> and Christopher J. Chang<sup>\*,†,‡</sup>

<sup>†</sup>Department of Chemistry and the <sup>‡</sup>Howard Hughes Medical Institute, University of California, Berkeley, California 94720, United States

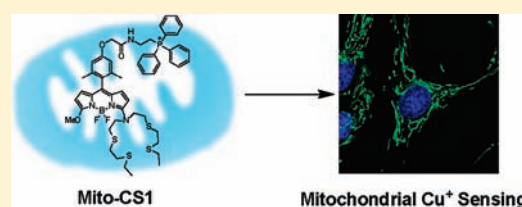
<sup>§</sup>Department of Biochemistry, University of Saskatchewan, Saskatoon, SK S7N 5E5, Canada

<sup>||</sup>Department of Biological Sciences, Auburn University, Auburn, Alabama 36849, United States

<sup>⊥</sup>Department of Medicine and Biochemistry, University of Utah Health Sciences Center, Salt Lake City, Utah 84132, United States

**S** Supporting Information

**ABSTRACT:** We present the design, synthesis, spectroscopy, and biological applications of Mitochondrial Coppersensor-1 (Mito-CS1), a new type of targetable fluorescent sensor for imaging exchangeable mitochondrial copper pools in living cells. Mito-CS1 is a bifunctional reporter that combines a Cu<sup>+</sup>-responsive fluorescent platform with a mitochondrial-targeting triphenylphosphonium moiety for localizing the probe to this organelle. Molecular imaging with Mito-CS1 establishes that this new chemical tool can detect changes in labile mitochondrial Cu<sup>+</sup> in a model HEK 293T cell line as well as in human fibroblasts. Moreover, we utilized Mito-CS1 in a combined imaging and biochemical study in fibroblasts derived from patients with mutations in the two synthesis of cytochrome *c* oxidase 1 and 2 proteins (*SCO1* and *SCO2*), each of which is required for assembly and metalation of functionally active cytochrome *c* oxidase (COX). Interestingly, we observe that although defects in these mitochondrial metallochaperones lead to a global copper deficiency at the whole cell level, total copper and exchangeable mitochondrial Cu<sup>+</sup> pools in *SCO1* and *SCO2* patient fibroblasts are largely unaltered relative to wild-type controls. Our findings reveal that the cell maintains copper homeostasis in mitochondria even in situations of copper deficiency and mitochondrial metallochaperone malfunction, illustrating the importance of regulating copper stores in this energy-producing organelle.



## INTRODUCTION

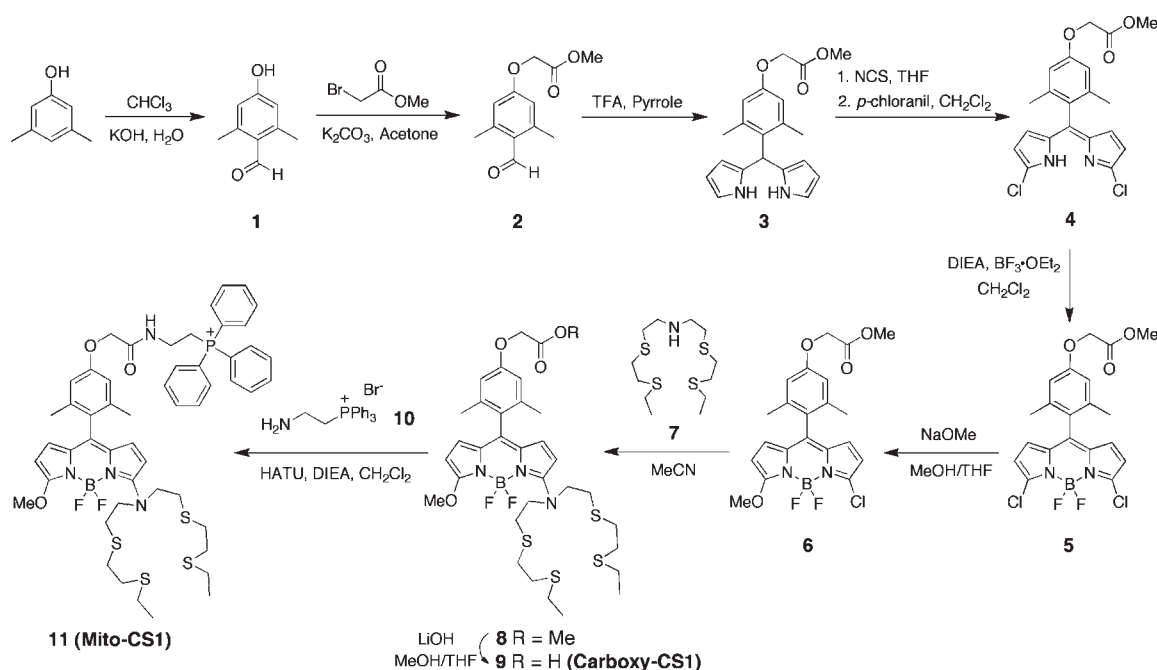
Copper is a required element for life, and regulating its uptake, efflux, and compartmentalization at the cellular level is vital for maintaining normal physiology.<sup>1–3</sup> As such, cells have evolved intricate mechanisms that coordinate the activity of transporters, chaperones, and small-molecule ligands to dynamically control the distribution of copper within discrete subcellular spaces.<sup>4–24</sup> In this context, mitochondria are important reservoirs for cellular copper due to the essential role of this metal ion as a cofactor for the respiratory enzyme cytochrome *c* oxidase (COX), which reduces oxygen to water in the terminal step of aerobic respiration.<sup>25–30</sup> In addition to the copper present in COX, mitochondria utilize this metal ion as a cofactor for superoxide dismutase (SOD1) contained within the mitochondrial intermembrane space (IMS), and a matrix-localized pool of copper is relocated to the IMS to metalate both of these enzymes.<sup>31</sup> Assembly of active COX in mitochondria requires a host of proteins, including the two synthesis of cytochrome *c* oxidase genes (*SCO1* and *SCO2*) that collectively mediate a series of metal- and redox-dependent events crucial for COX metalation and holoenzyme maturation.<sup>32–44</sup> Mutations in either of the SCO chaperones result in severe, tissue-specific clinical phenotypes that are caused by both a failure to mature functionally active COX for aerobic respiration and an inability to appropriately regulate cellular copper homeostasis.<sup>36,45–59</sup>

Because regulating mitochondrial copper homeostasis is critical to maintaining central oxygen metabolism in the cell, new chemical tools that allow direct, real-time visualization of exchangeable mitochondrial copper pools in living samples are potentially powerful reagents with which to directly investigate the spatiotemporal distribution of this redox-active metal in both healthy and diseased states. Toward this end, we have initiated a broad-based program to create fluorescent and MRI agents for monitoring labile copper stores in living systems.<sup>60–68</sup> Previous work from our laboratory on fluorescent sensors for live-cell copper imaging includes intensity and ratiometric probes Coppersensor-1 (CS1),<sup>60,61</sup> Coppersensor-3 (CS3),<sup>68</sup> and Ratio-Coppersensor-1 (RCS1),<sup>67</sup> which are capable of selectively tracking labile cellular Cu<sup>+</sup> stores with metal and/or redox stimulation. However, these first-generation sensors and other elegant examples of small molecule or protein-based copper sensors<sup>69–71</sup> are not preferentially directed to mitochondria or other organelles, which offers an opportunity to devise new probes that can be targeted to discrete subcellular compartments for imaging local changes in the abundance/availability of exchangeable Cu<sup>+</sup>.

Received: January 15, 2011

Published: May 12, 2011

Scheme 1



In this Article, we present the design, synthesis, spectroscopy, and biological applications of Mitochondrial Coppersensor-1 (Mito-CS1), a new type of fluorophore for imaging dynamic mitochondrial copper stores in living cells with metal ion and spatial specificity (Scheme 1). Mito-CS1 can reversibly detect endogenous, exchangeable mitochondrial  $\text{Cu}^+$  pools in a model HEK 293T cell line as well as in cultured human fibroblasts. Moreover, we apply Mito-CS1 in a combined molecular imaging and biochemical study to investigate mitochondrial copper homeostasis in fibroblasts derived from patients with *SCO1* and *SCO2* mutations. Interestingly, the data establish that, although loss of function mutations in *SCO1* and *SCO2* causes a severe, global copper deficiency at the whole cell level, both the exchangeable  $\text{Cu}^+$  and the total mitochondrial copper pools are only mildly perturbed in *SCO1* and *SCO2* patient fibroblasts as compared to wild-type congeners. Our results show that the cell maintains the homeostatic regulation of copper within mitochondria, even when faced with a globally severe state of copper deficiency, and underscore the primary importance of this redox-active metal in central metabolism and cellular energy homeostasis.<sup>72</sup>

## RESULTS AND DISCUSSION

**Design and Synthesis of a Targetable Coppersensor Platform and Preparation of Mito-CS1.** To monitor labile mitochondrial copper pools in living cells by real-time fluorescence imaging, we designed a bifunctional BODIPY dye that contains both a fluorescence-responsive  $\text{Cu}^+$ -binding domain and a mitochondrial-targeting moiety. For the latter, we exploited phosphonium head groups that have been pioneered by Murphy<sup>73–76</sup> and subsequently utilized by ourselves<sup>77,78</sup> and others<sup>79–84</sup> to selectively direct attached cargo to mitochondria via their proton gradients. In addition, we designed a synthetic pathway that builds up to one key intermediate, Carboxy-CS1, which combines a BODIPY chromophore, a thioether-rich receptor for selective recognition and binding of  $\text{Cu}^+$ , and a carboxylic acid synthetic handle (Scheme 1, compound 9) for facile introduction of a

triphenylphosphonium tag or any other desired targeting functionality. We note that modification of the BODIPY chromophore to incorporate additional functionalities has been explored in the literature.<sup>85,86</sup>

Scheme 1 outlines the synthesis of Mito-CS1. Briefly, alkylation of aldehyde 1 with methyl bromoacetate furnishes the methyl ester 2 in 58% yield. Condensation of 2 with excess pyrrole and catalytic trifluoroacetic acid affords dipyrromethane 3 in 19% yield. Subsequent chlorination followed by oxidation with *p*-chloranil gives the dichloro dipyrromethane 4 in 44% yield over two steps; because isolation of the putative dichloro dipyrromethane intermediate is low yielding, we found that a halogenation/oxidation protocol was more synthetically tractable. Boron insertion with  $\text{BF}_3 \cdot \text{OEt}_2$  generates the dichloro BODIPY 5 in 75% yield. Nucleophilic displacement with sodium methoxide yields 6, which is then coupled to the azatetrathia receptor 7 to generate 8 in 56% yield. Ester hydrolysis of 8 under basic conditions yields Carboxy-CS1 9. Peptide coupling of 9 and the mitochondrial-targeted tag 10 with HATU delivers Mito-CS1 (11) in 48% yield. We note that these mild and robust coupling conditions allow for the potential introduction of other functional tags onto Carboxy-CS1, including ones that can be used to direct fluorescent copper sensors to other organelles and other subcellular targets, and that the synthetic pathway toward Mito-CS1 generates a versatile set of precursor materials (compounds 3, 4, 5, and 6).

**Spectroscopic Properties of Mito-CS1.** The spectroscopic properties of Mito-CS1 were evaluated in aqueous media buffered to physiological pH (PBS, pH 7.4). Apo Mito-CS1 features one prominent optical band at 555 nm ( $\epsilon = 2.8 \times 10^4 \text{ M}^{-1} \text{ cm}^{-1}$ ) with a shoulder at 520 nm and a corresponding emission maximum at 569 nm with weak fluorescence ( $\Phi = 0.009$ ). Upon addition of  $\text{Cu}^+$ , the absorption spectrum of  $\text{Cu}^+$ -bound Mito-CS1 displays a single major visible absorption band at 550 nm ( $\epsilon = 2.6 \times 10^4 \text{ M}^{-1} \text{ cm}^{-1}$ ). The fluorescence intensity of Mito-CS1 increases by ca. 10-fold ( $\Phi = 0.05$ , Figure 1a) with a slight blue shift of the emission maximum to 558 nm with 1 equiv of  $\text{Cu}^+$  added

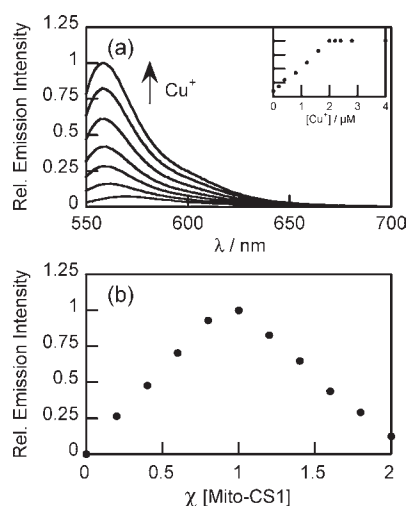


**Figure 1.** Mito-CS1 responds to  $\text{Cu}^+$  in an aqueous solution with 1:1 binding. (a) Fluorescence response of  $2 \mu\text{M}$  Mito-CS1 to  $\text{Cu}^+$ . Spectra shown are for  $\text{Cu}^+$  concentrations of 0, 0.2, 0.4, 0.8, 1.2, 1.6, 2.0, 2.2, 2.4, 2.8, and  $4 \mu\text{M}$ . Spectra were acquired in PBS, pH 7.4, with 540 nm excitation. Inset: Normalized fluorescence response ( $y$ -axis) of  $2 \mu\text{M}$  Mito-CS1 to  $\text{Cu}^+$ . Spectra were acquired in PBS, pH 7.4. Excitation was provided at 540 nm, and the integrated emission was collected from 550–700 nm. (b) Normalized Job's plot of Mito-CS1 and  $\text{Cu}^+$ . The total concentration of Mito-CS1 and  $\text{Cu}^+$  was kept constant at  $2 \mu\text{M}$ . Spectra were acquired in PBS, pH 7.4. Excitation was provided at 540 nm, and emission intensity was measured at 558 nm.

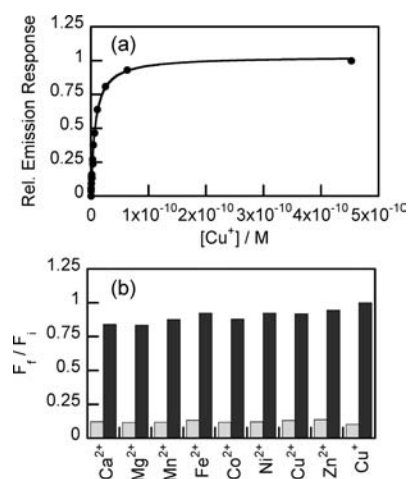


**Figure 2.** Mito-CS1 can respond to a dynamic range of  $\text{Cu}^+$  concentrations and is selective for  $\text{Cu}^+$  over other biologically relevant metal ions. (a) Normalized fluorescence responses of  $2 \mu\text{M}$  Mito-CS1 to thiourea buffered  $\text{Cu}^+$  solutions for  $K_d$  value determination. Spectra were acquired in PBS, pH 7.4. Excitation was provided at 540 nm, and the collected emission was integrated over 550–700 nm. The points shown are for free  $\text{Cu}^+$  buffered at 0.10, 0.21, 0.45, 0.72, 0.91, 1.3, 1.4, 2.6, 3.0, 3.8, 6.1, 10.9, 25.1, 63.1, and  $452.5 \text{ pM}$ , respectively. The observed  $K_d$  value is  $7.2(3) \times 10^{-12} \text{ M}$ . (b) Fluorescence responses of  $2 \mu\text{M}$  Mito-CS1 to various metal ions. Bars represent the final ( $F_f$ ) over the initial ( $F_i$ ) integrated emission. Gray bars represent the addition of the competing metal ion ( $2 \text{ mM}$  for  $\text{Ca}^{2+}$  and  $\text{Mg}^{2+}$ ,  $500 \mu\text{M}$  for  $\text{Zn}^{2+}$ , and  $50 \mu\text{M}$  for all other cations) to a  $2 \mu\text{M}$  solution of Mito-CS1. Black bars represent the addition of  $2 \mu\text{M}$   $\text{Cu}^+$  to the solution. Spectra were acquired in PBS, pH 7.4. Excitation was provided at 540 nm, with emission integrated over 550–700 nm.

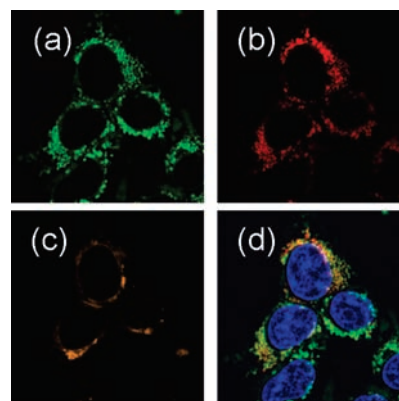


**Figure 3.** Mito-CS1 colocalizes to mitochondria in live HEK 293T cells. HEK cells were stained with (a) 500 nM Mito-CS1, (b) 50 nM MitoTracker Deep Red, and (c)  $2.25 \mu\text{M}$  BODIPY FL C5-ceramide-BSA complex and  $5 \mu\text{M}$  Hoechst 33342 for 15 min at  $37^\circ\text{C}$  in DPBS. (d) Overlay of (a) and (b) with Hoechst 33342.

(Figure 1a, inset), similar in photochemical properties to the previously reported turn-on fluorescent sensor CS1<sup>60</sup> ( $\text{Cu}^+$ -bound  $\Phi = 0.13$ , 10-fold turn-on response) but with the added functionality of a targeting phosphonium moiety. Binding analysis using the method of continuous variations (Job's plot) indicates a 1:1  $\text{Cu}^+$ :dye complex is responsible for the observed fluorescence enhancement (Figure 1b). These results demonstrate that Mito-CS1 can dynamically respond to changes in  $\text{Cu}^+$  levels in aqueous media. The apparent  $K_d$  for the Mito-CS1: $\text{Cu}^+$  complex is  $7.2(3) \times 10^{-12} \text{ M}$  in PBS buffer at pH 7.4 (Figure 2a). Even in the presence of a lipophilic phosphonium cation, Mito-CS1 maintains its high selectivity for  $\text{Cu}^+$  over other biologically relevant metal ions (Figure 2b). The fluorescence response of apo or  $\text{Cu}^+$ -bound Mito-CS1 is not affected by the presence of physiologically relevant concentrations of  $\text{Ca}^{2+}$ ,  $\text{Mg}^{2+}$ , and  $\text{Zn}^{2+}$ . Moreover, other bioavailable divalent metal ions ( $\text{Mn}^{2+}$ ,  $\text{Fe}^{2+}$ ,  $\text{Co}^{2+}$ ,  $\text{Ni}^{2+}$ ,  $\text{Cu}^{2+}$ ) do not induce a change in the emission intensity of the apo probe and do not interfere with the  $\text{Cu}^+$  response. Finally, Mito-CS1 is selective for  $\text{Cu}^+$  over  $\text{Cu}^{2+}$ , showing that this probe has metal and redox specificity.

**Fluorescence Detection of a Labile Mitochondrial  $\text{Cu}^+$  Pool in HEK 293T Cells Using Mito-CS1.** With spectroscopic data establishing that Mito-CS1 can selectively respond to  $\text{Cu}^+$  in aqueous solution, we turned our attention to evaluate Mito-CS1 in live-cell imaging assays using HEK 293T as a model cell line. First, we tested Mito-CS1 for its ability to localize to mitochondria. Accordingly, HEK 293T cells stained with 500 nM Mito-CS1 for 15 min at  $37^\circ\text{C}$  show measurable levels of fluorescence in discrete subcellular locations as determined by confocal microscopy (Figure 3a, Figure S1a). Co-staining experiments with MitoTracker Deep Red, a commercially available mitochondrial tracker (Figure 3b), BODIPY FL C5-ceramide, a marker for the trans-Golgi (Figure 3c), and LysoTracker Green DND-26, a lysosomal marker (Figure S1b), establish that the observed fluorescence from Mito-CS1 is localized to mitochondria in these live cells. Furthermore, nuclear staining with Hoechst 33342 indicates that the cells are viable throughout the imaging experiments (Figure 3d, Figure S1c).

We next tested whether Mito-CS1 was sensitive enough to detect basal levels of labile mitochondrial  $\text{Cu}^+$  and whether it could respond to increases and/or decreases in the size of this pool. First, HEK 293T cells were cultured in growth media only

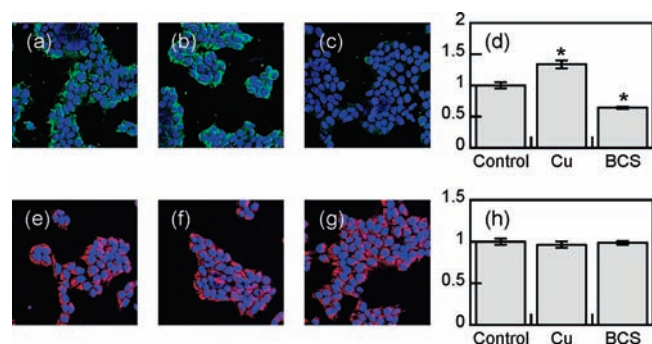


**Figure 4.** Live-cell molecular imaging with Mito-CS1 and Rhodamine 123 reveals a labile mitochondrial Cu<sup>+</sup> pool in HEK 293T Cells. (a) Control HEK cells, (b) HEK cells supplemented with 300 μM CuCl<sub>2</sub> in the growth medium for 18 h at 37 °C, and (c) HEK cells supplemented with 100 μM BCS in the growth medium for 18 h at 37 °C were stained with 500 nM Mito-CS1 and 5 μM Hoechst 33342 for 15 min at 37 °C in DPBS. (d) Plot of the mean fluorescence intensity of (a)–(c). Data were normalized to the control, and statistical analyses were performed with a two-tailed Student's *t*-test ( $n = 4$  fields of cells) relative to the control. \* $P < 0.01$  and error bars are  $\pm$ sem. (e) Control HEK cells, (f) HEK cells supplemented with 300 μM CuCl<sub>2</sub> in the growth medium for 18 h at 37 °C, and (g) HEK cells supplemented with 100 μM BCS in the growth medium for 18 h at 37 °C were stained with 100 nM Rhodamine 123 and 5 μM Hoechst 33342 for 15 min at 37 °C in DPBS. (h) Plot of the mean fluorescence intensity of (e)–(g). Data were normalized to the control, statistical analyses were performed with a two-tailed Student's *t*-test ( $n = 4$  fields of cells) relative to the control, and error bars are  $\pm$ sem.

or growth media supplemented with 300 μM CuCl<sub>2</sub> for 18 h to globally elevate intracellular copper stores and subsequently imaged by confocal microscopy (Figure 4a,b). As visualized by Mito-CS1, we observe that exchangeable mitochondrial Cu<sup>+</sup> levels rise by 34% with copper supplementation relative to control, indicating that Mito-CS1 can detect expansions in the mitochondrial Cu<sup>+</sup> pool (Figure 4d).<sup>31</sup> To evaluate whether Mito-CS1 can also report on decreases in exchangeable mitochondrial Cu<sup>+</sup> levels, HEK 293T cells were cultured in growth media only or growth media supplemented with 100 μM of the membrane-impermeable Cu<sup>+</sup> chelator bathocuproine disulfonate (BCS) for 18 h to globally deplete intracellular copper stores,<sup>87</sup> and each set of cells were then stained with Mito-CS1 and imaged by confocal microscopy. Upon addition of BCS, labile mitochondrial Cu<sup>+</sup> levels decrease by 36% relative to basal Cu<sup>+</sup> levels (Figure 4a,c), showing that Mito-CS1 can image basal levels of mitochondrial Cu<sup>+</sup> and detect depletions in this pool. In addition, nuclear staining with Hoechst 33342 confirms that the viability of HEK 293T cells is unaffected by the manipulation of cellular copper status (Figure 4a–c).

Finally, as an additional set of controls to corroborate that Mito-CS1 is detecting copper-dependent events, we performed analogous imaging studies with Rhodamine 123, a well-established fluorescent marker for assaying mitochondrial membrane potential,<sup>88,89</sup> under basal, copper-supplemented, and copper-depleted conditions. As described above, endogenous copper pools of HEK 293T cells were elevated with supplementation or depleted with chelation and then stained with 100 nM Rhodamine 123 (Figure 4e–g). The membrane potential as measured by Rhodamine 123 does not show statistically significant changes with either 300 μM CuCl<sub>2</sub> or 100 μM BCS treatment relative to control HEK 293T cells (Figure 4h), providing further evidence

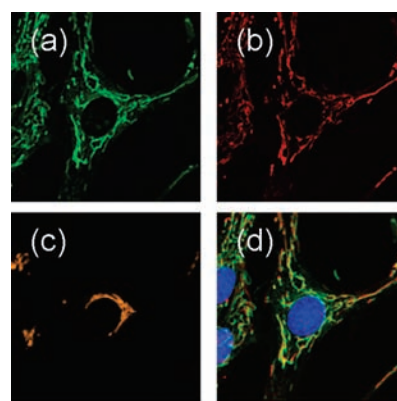


**Figure 5.** Live-cell molecular imaging shows that Mito-CS1 colocalizes to mitochondria in a control cell line derived from human fibroblasts. Control fibroblasts were stained with (a) 5 μM Mito-CS1, (b) 50 nM MitoTracker Deep Red, and (c) 2.25 μM BODIPY FL C<sub>5</sub>-ceramide-BSA complex and 5 μM Hoechst 33342 for 15 min at 37 °C in DPBS. (d) Overlay of (a) and (b) with Hoechst 33342.

that Mito-CS1 is sensing changes in labile mitochondrial copper pools rather than reporting on mitochondrial membrane potential.

#### Mito-CS1 Imaging and ICP-OES Experiments Reveal that Mitochondrial Cu<sup>+</sup> Pools in *SCO1* and *SCO2* Patient Fibroblasts Are Comparable to Wild-type Counterparts.

In our first application of Mito-CS1 as an analytical tool, we investigated whether the labile and total mitochondrial copper pools are affected by mutations in *SCO1* and *SCO2*, which are known to cause a severe copper deficiency at the cellular level in affected tissues and cell types.<sup>36</sup> We first evaluated the ability of Mito-CS1 to localize to mitochondria in human fibroblasts. As seen with HEK 293T cells, confocal microscopy of control fibroblasts stained with 5 μM Mito-CS1 for 15 min at 37 °C shows measurable levels of fluorescence in discrete subcellular locations (Figure 5a, Figure S2a). Co-staining experiments with MitoTracker Deep Red, a commercially available mitochondrial tracker (Figure 5b), BODIPY FL C<sub>5</sub>-ceramide, a marker for the trans-Golgi (Figure 5c), and LysoTracker Green DND-26, a lysosomal marker (Figure S2b), establish that the observed fluorescence from Mito-CS1 is localized to mitochondria of these cells. Furthermore, nuclear staining with Hoechst 33342 indicates that the cells are viable throughout the imaging experiments (Figure 5d, Figure S2c).

Analogous to the HEK 293T cells, we next tested how changes in global copper status affect the exchangeable mitochondrial copper pool in control fibroblasts. Control fibroblasts were grown in media supplemented with 300 μM and 500 μM CuCl<sub>2</sub> for 18 h and then stained with 5 μM Mito-CS1 for 15 min at 37 °C. The labile mitochondrial Cu<sup>+</sup> pool as visualized by Mito-CS1 is significantly expanded upon coculture of fibroblasts with 500 μM CuCl<sub>2</sub> (Figure S3a–c). Staining with Rhodamine 123 does not show a statistically significant difference in the membrane potential between untreated and copper-supplemented fibroblasts (Figure S3d–f). Control fibroblasts treated with 100 μM BCS for 12 h and then stained with 5 μM Mito-CS1 for 15 min at 37 °C show a 45% decrease in mitochondrially localized fluorescence intensity as compared to their untreated counterparts (Figure 6a–c). The observed decrease in fluorescence intensity of Mito-CS1 in BCS-treated fibroblasts demonstrates that these cells possess a dynamic mitochondrial Cu<sup>+</sup> pool that is affected by changes in global copper status. In a set of parallel control experiments, Rhodamine 123 staining of control

fibroblasts grown in normal media or media with 100  $\mu\text{M}$  BCS for 12 h reveals no differences in membrane potential (Figure 6d–f), and nuclear staining with Hoechst 33342 shows that the cells are

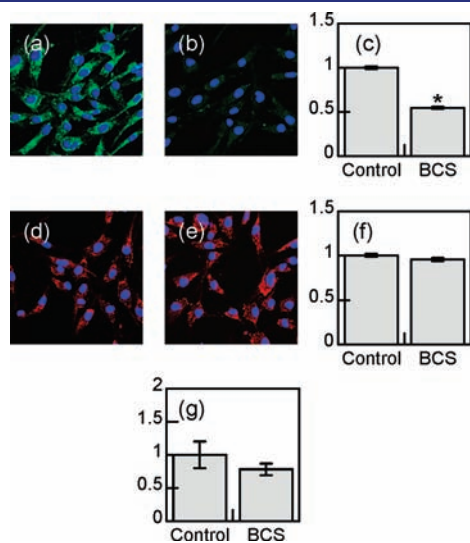


**Figure 6.** Live-cell molecular imaging with Mito-CS1 and Rhodamine 123, biochemical approaches, and elemental analyses reveal that there is a dynamic mitochondrial  $\text{Cu}^+$  pool in a control cell line derived from human fibroblasts. (a) Control fibroblasts, and (b) control fibroblasts supplemented with 100  $\mu\text{M}$  BCS in the growth medium for 12 h at 37  $^{\circ}\text{C}$  were stained with 5  $\mu\text{M}$  Mito-CS1 and 5  $\mu\text{M}$  Hoechst 33342 for 15 min at 37  $^{\circ}\text{C}$  in DMEM. (c) Plot of the mean fluorescence intensity of (a) and (b). Data were normalized to the control, and statistical analyses were performed with a two-tailed Student's *t*-test ( $n = 5$  fields of cells). \* $P < 0.01$  and error bars are  $\pm\text{sem}$ . (d) Control fibroblasts and (e) control fibroblasts supplemented with 100  $\mu\text{M}$  BCS in the growth medium for 12 h at 37  $^{\circ}\text{C}$  were stained with 100 nM Rhodamine 123 and 5  $\mu\text{M}$  Hoechst 33342 for 15 min at 37  $^{\circ}\text{C}$  in DMEM. (f) Plot of the mean fluorescence intensity of (d) and (e). Data were normalized to the control, statistical analyses were performed with a two-tailed Student's *t*-test ( $n = 5$  fields of cells), and error bars are  $\pm\text{sem}$ . (g) COX activity<sup>32,97</sup> was measured in control fibroblasts and control fibroblasts supplemented with 100  $\mu\text{M}$  BCS in the growth medium for 24 h. Data were normalized to the control, statistical analyses were performed with a two-tailed Student's *t*-test ( $n = 3$ ), and error bars are  $\pm\text{sem}$ .

viable throughout the BCS treatment and imaging experiments (Figure 6a–d). COX activity is mildly reduced with 100  $\mu\text{M}$  BCS treatment for 24 h (Figure 6g) but not sufficiently to affect the membrane potential (Figure 6e). Taken together, the data further establish that Mito-CS1 directly detects and responds to changes in endogenous mitochondrial  $\text{Cu}^+$  levels in cultured human fibroblasts.

After establishing that Mito-CS1 can monitor the labile mitochondrial  $\text{Cu}^+$  pool in control fibroblasts and sense dynamic changes in its size with alterations in copper status, we used this new chemical tool to characterize mitochondrial  $\text{Cu}^+$  homeostasis in fibroblasts derived from patients with mutations in *SCO1* and *SCO2*. We also included fibroblasts derived from a patient with mutations in the copper exporter protein *ATP7A* in our analyses, for loss of *ATP7A* function in this cell type results in significant increases in total cellular copper content.<sup>90,91</sup> Control, *SCO1*, *SCO2*, and *ATP7A* patient fibroblasts were cultured for 48 h in growth medium, stained with 5  $\mu\text{M}$  Mito-CS1 in DMEM, and imaged live by scanning confocal microscopy. Consistent with our findings using control fibroblasts, mutations in *ATP7A*, *SCO1*, and *SCO2* do not affect the mitochondrial localization of Mito-CS1 or overall cell viability (Figure 7a–d). Interestingly, quantification of the Mito-CS1 fluorescence intensities reveals that the size of the labile mitochondrial  $\text{Cu}^+$  pool is comparable in control, *SCO1*, and *SCO2* patient fibroblasts, while it is significantly expanded in *ATP7A* patient fibroblasts (Figure 7e). We next used ICP-OES to measure total Cu at the whole cell and mitochondrial levels of organization in all four genetic backgrounds (Figure 7f). As expected, total cellular copper content is elevated in *ATP7A* patient fibroblasts and decreased in *SCO1* and *SCO2* patient fibroblasts when compared to control fibroblasts. In contrast, the total mitochondrial copper pool is only modestly altered in the patient backgrounds (Figure 7g), illustrating that this organelle more tightly controls its total and labile copper pools relative to the whole cell. Because the majority of mitochondrial copper is housed in the matrix and previous studies with competitor proteins, *in vitro* titrations, and targeted chelators<sup>31,69</sup> argue that this pool is exchangeable, Mito-CS1 is likely visualizing this store within living cells. We performed two sets of additional control experiments to further support that Mito-CS1 is specifically reporting on a  $\text{Cu}^+$ -sensitive phenomenon in these patient fibroblasts. First, we used Rhodamine 123 staining to demonstrate that the mitochondrial

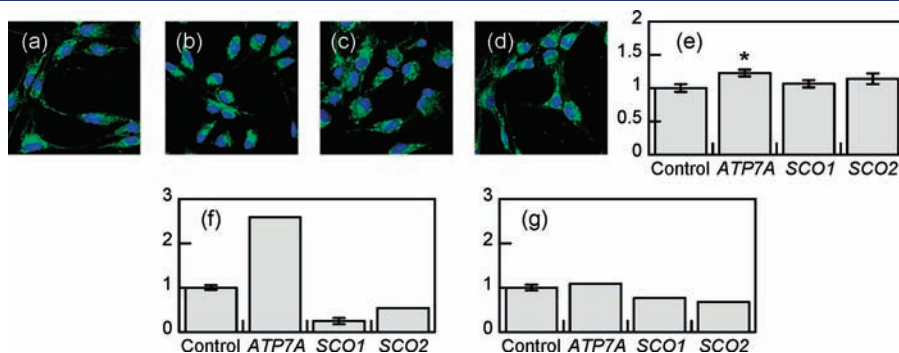


**Figure 7.** Live-cell molecular imaging with Mito-CS1, biochemical approaches, and bulk metal ion analyses confirm that mutations in *SCO1* and *SCO2* do not significantly perturb the mitochondrial copper homeostasis. (a) Control fibroblasts, (b) *ATP7A* patient fibroblasts, (c) *SCO1* patient fibroblasts, and (d) *SCO2* patient fibroblasts were stained with 5  $\mu\text{M}$  Mito-CS1 and 5  $\mu\text{M}$  Hoechst 33342 for 15 min at 37  $^{\circ}\text{C}$  in DMEM. (e) Plot of the mean fluorescence intensity of (a)–(d). Data were normalized to the control, and statistical analyses were performed with a two-tailed Student's *t*-test ( $n \geq 4$  fields of cells) relative to the control. \* $P < 0.05$ , and error bars are  $\pm\text{sem}$ . (f) Total copper levels were measured in control ( $n = 7$ ), *ATP7A*, *SCO1* ( $n = 6$ ), and *SCO2* patient fibroblasts, and (g) mitochondrial copper levels were measured in control ( $n = 4$ ), *ATP7A*, *SCO1*, and *SCO2* patient fibroblasts by ICP-OES and are expressed as a fraction of the control using a previously described procedure.<sup>36</sup>

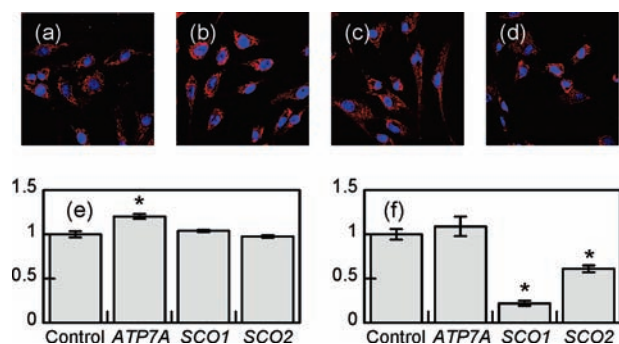


**Figure 8.** Live-cell molecular imaging with Rhodamine 123 and biochemical approaches reveal that the membrane potential is preserved in COX-deficient fibroblasts derived from *SCO1* and *SCO2* patients. (a) Control, (b) *ATP7A*, (c) *SCO1*, and (d) *SCO2* patient fibroblasts were stained with 50 nM Rhodamine 123 and 5  $\mu$ M Hoechst 33342 for 15 min at 37 °C in DMEM. (e) Plot of the mean fluorescence intensity of (a)–(d). Data were normalized to the control, and statistical analyses were performed with a two-tailed Student's *t*-test ( $n \geq 4$  fields of cells) relative to the control. \* $P < 0.01$  and error bars are  $\pm$ sem. (f) COX activity was measured in control, *ATP7A*, *SCO1*, and *SCO2* fibroblasts using a previously described procedure.<sup>32,97</sup> Data were normalized to the control, and statistical analyses were performed with a two-tailed Student's *t*-test ( $n = 3$ ) relative to the control. \* $P < 0.01$  and error bars are  $\pm$ sem.

membrane potential is maintained in both *SCO1* and *SCO2* patient backgrounds relative to the control (Figure 8a–e). Second, we measured COX activity in fibroblasts from all four genetic backgrounds (Figure 8f) to confirm the presence of a severe COX deficiency in fibroblasts lacking functional *SCO1* or *SCO2*. The collective data show that the observed changes in Mito-CS1 fluorescence are copper-dependent and are not an indirect consequence or nonspecific phenomenon of differences across the cell lines in COX activity and/or membrane potential.

Finally, to support that the data obtained from *SCO1* and *SCO2* patient fibroblasts are representative of the observed *in vivo* phenotypes, we measured total copper content in crude mitochondria isolated from control, *SCO1*, and *SCO2* patient livers by ICP-OES (Figure S4). As in cultured fibroblasts, the data show that the mitochondrial copper pool is not significantly altered in liver as a result of mutations in *SCO1* or *SCO2* (Figure S3a). While there was considerable variability in mitochondrial copper content across control liver samples, this observation can be explained by differences in total hepatocyte copper content (Figure S3b). Comparable copper levels in crude and highly purified mitochondria isolated from HEK 293T cells further suggest that the variation in mitochondrial copper levels observed across control liver samples is not simply a consequence of the isolation procedure (Figure S3a). Therefore, consistent with previously reported results,<sup>36</sup> these data further suggest that fibroblasts are a competent disease model in terms of copper misregulation. Taken together, the combination of Mito-CS1 imaging and ICP-OES measurements patently shows that the mitochondrial copper store is a tightly regulated metal ion pool, as we observe little to no perturbation in the labile mitochondrial  $\text{Cu}^+$  and total mitochondrial copper pools in *ATP7A*, *SCO1*, and *SCO2* patient fibroblasts as compared to control congeners.

## CONCLUDING REMARKS

In this Article, we have described the synthesis, properties, and biological applications of Mito-CS1, a new targetable fluorescent

probe that can selectively detect labile  $\text{Cu}^+$  in mitochondria of living cells. Mito-CS1 is a unique  $\text{Cu}^+$ -specific small-molecule fluorescent indicator that features visible excitation and emission profiles, a turn-on response, and selectivity for  $\text{Cu}^+$  over other abundant mitochondrial metal ions, including  $\text{Fe}^{2+}$ ,  $\text{Cu}^{2+}$ , and  $\text{Zn}^{2+}$ . Confocal microscopy experiments with a model HEK 293T cell line and human fibroblasts establish that Mito-CS1 is chemically and spatially specific within living cells for mitochondrial  $\text{Cu}^+$ . Furthermore, we used Mito-CS1 in conjunction with biochemical and ICP metal analyses to monitor mitochondrial copper pools in *SCO* and *ATP7A* patient fibroblasts, cell lines that exhibit profound alterations in total cellular copper levels that mirror those observed in affected patient tissues *in vivo*. Interestingly, these experiments show that the mutations in question do not dramatically alter labile mitochondrial  $\text{Cu}^+$  or total mitochondrial Cu pools relative to control cells, suggesting that cells maintain homeostatic control over mitochondria regulating copper homeostasis within a narrow window, to protect the main oxygen-consuming and energy-producing organelle relative to other areas of the cell. We anticipate that the Mito-CS1 reagent will find utility for future interrogations of how discrete copper handling pathways are organized into dynamic networks at the cell and systems levels of organization. In addition to applying Mito-CS1 for studies of mitochondrial copper biology, we are exploiting the modular probe scaffold to create new multifunctional probes for detecting  $\text{Cu}^+$  and other biologically relevant analytes in discrete subcellular locales.

## EXPERIMENTAL SECTION

**Synthetic Materials and Methods.** All reactions were carried out under a dry nitrogen atmosphere with flame-dried glassware. Silica gel P60 (SiliCycle) was used for column chromatography. Analytical thin layer chromatography was performed using SiliCycle 60 F254 silica gel (precoated sheets, 0.25 mm thick). Compound **1**,<sup>92</sup> compound **10**,<sup>93</sup> and Rhodamine 123<sup>94</sup> were synthesized according to modified literature procedures. Compound **7**<sup>60,61</sup> was prepared according to previously reported procedures. HATU was purchased from ChemPep Inc. (Wellington, FL). MitoTracker Deep Red, BODIPY FL  $\text{C}_5$ -ceramide, LysoTracker DND-26, and Hoechst 33342 were purchased from Invitrogen (Carlsbad, CA). All other chemicals were purchased from Sigma-Aldrich (St. Louis, MO) and were used as received.  $^1\text{H}$  and  $^{13}\text{C}$  NMR spectra were collected in  $\text{CDCl}_3$ ,  $\text{CD}_3\text{OD}$ , and  $(\text{CD}_3)_2\text{SO}$  (Cambridge Isotope Laboratories, Cambridge, MA) at 25 °C on a Bruker AVB-400 spectrometer at the College of Chemistry NMR Facility at the University of California, Berkeley. All chemical shifts are reported in the standard notation of parts per million using the peak of residual proton signals of  $\text{CDCl}_3$  as an internal reference. Low-resolution mass spectral analyses were carried out using a 6130 quadrupole LC/MS 1200 Series (Agilent Technologies, Santa Clara, CA). High-resolution mass spectral analyses were carried out at the College of Chemistry Mass Spectrometry Facility at the University of California, Berkeley.

**4-Hydroxy-2,6-dimethylbenzaldehyde (1).** Compound **1** was prepared according to a previously reported procedure with the following modifications:  $\text{CHCl}_3$  was passed over alumina and then added dropwise over 30 min to the reaction mixture. Characterization was consistent with that previously reported in the literature.<sup>92</sup>

**Methyl 2-(4-Formyl-3,5-dimethylphenoxy)acetate (2).** Methyl 2-bromoacetate (3.8 mL, 40 mmol) in anhydrous MeCN (60 mL) was added dropwise to a suspension of compound **1** (5.0 g, 33.3 mmol) and  $\text{K}_2\text{CO}_3$  (9.19 g, 66.6 mmol) in MeCN (50 mL) at 60 °C. The resulting solution was heated at 60 °C for 2 days. The

reaction mixture was cooled to room temperature and concentrated *in vacuo*. The crude reaction mixture was partitioned between water (100 mL) and EtOAc (3 × 100 mL). The organics were combined, dried over Na<sub>2</sub>SO<sub>4</sub>, filtered, and dried *in vacuo*. Diethyl ether (50 mL) was added to the crude solid, and the resulting solid was collected via vacuum filtration and washed with diethyl ether (50 mL) to furnish compound **2** as an off-white solid (4.31 g, 58%). The reaction was repeated to generate more material for the subsequent reactions. <sup>1</sup>H NMR (400 MHz, CDCl<sub>3</sub>): δ 2.59 (6H, s), 3.81 (3H, s), 6.58 (2H, s), 10.46 (1H, s). <sup>13</sup>C NMR (100 MHz, CDCl<sub>3</sub>): δ 21.1, 52.5, 64.8, 115.3, 126.9, 144.6, 160.7, 168.8, 191.7. LRESI-MS calculated for [MH<sup>+</sup>] 223.1, found 223.1.

**Methyl 2-(4-(Di(1H-pyrrol-2-yl)methyl)-3,5-dimethylphenoxy)acetate (3)**. A solution of **2** (6.38 g, 28.7 mmol) in freshly distilled pyrrole (50.0 mL, 721 mmol) was wrapped in foil to protect it from light and purged with a stream of N<sub>2</sub> for 5 min. TFA (240 μL, 5.4 mmol) was then added dropwise, and the solution was stirred at room temperature for 1 h. After 1 h, TEA (1.0 mL, 7.2 mmol) was added, and the reaction mixture continued to stir for 15 min. The reaction mixture was poured into toluene (150 mL) and washed with brine (2 × 100 mL). The organics were combined, dried over Na<sub>2</sub>SO<sub>4</sub>, filtered, concentrated to dryness, and purified by flash chromatography two times (first column, silica CHCl<sub>3</sub> to 0.1% MeOH in CHCl<sub>3</sub>; second column, silica, 0.5% EtOAc in CH<sub>2</sub>Cl<sub>2</sub>) to give a crude solid. Diethyl ether was added (3 × 20 mL), decanted, and the solid was collected via vacuum filtration and washed with diethyl ether (40 mL) to yield **3** as an off-white solid (1.81 g, 19%). <sup>1</sup>H NMR (400 MHz, CDCl<sub>3</sub>): δ 2.08 (6H, s), 3.83 (3H, s), 4.62 (2H, s), 5.89 (1H, s), 5.99 (2H, br), 6.18 (2H, q, J = 2.8 Hz), 6.60 (2H, s), 6.67 (2H, br m), 7.97 (2H, s). <sup>13</sup>C NMR (100 MHz, CDCl<sub>3</sub>): δ 21.0, 38.1, 52.3, 65.1, 106.6, 108.7, 115.4, 116.3, 131.1, 131.2, 139.5, 156.3, 169.6. LRESI-MS calculated for [MH<sup>+</sup>] 339.2, found 339.2.

**(Z)-Methyl 2-(4-((5-Chloro-1H-pyrrol-2-yl)(5-chloro-2H-pyrrol-2-ylidene)methyl)-3,5-dimethylphenoxy)acetate (4)**. A solution of **3** (1.76 g, 5.2 mmol) in anhydrous THF (67 mL) was wrapped in foil to protect it from light and cooled to -78 °C. *N*-Chlorosuccinimide (1.53 g, 11.5 mmol) in anhydrous THF (20 mL) was wrapped in foil to protect it from light and was added dropwise in two portions via an addition funnel over the course of 15 min. The reaction was stirred for an additional 2 h at -78 °C, capped, and then placed in the freezer (-20 °C) overnight. The crude reaction mixture was poured into water (100 mL) at 0 °C and then extracted with CH<sub>2</sub>Cl<sub>2</sub> (3 × 100 mL). The organics were combined, dried over Na<sub>2</sub>SO<sub>4</sub>, filtered, concentrated to dryness, and purified by flash chromatography (first column, silica, 5% hexanes in CH<sub>2</sub>Cl<sub>2</sub> to 5% MeOH in CH<sub>2</sub>Cl<sub>2</sub>; second column, silica, 20% hexanes in CH<sub>2</sub>Cl<sub>2</sub> to CH<sub>2</sub>Cl<sub>2</sub>) to provide the dichloro dipyrromethane as a crude red solid. This was carried onto the next step without further purification. *p*-Chloranil (1.30 g, 5.3 mmol) was added to a solution of the crude intermediate (1.05 g, 2.6 mmol) in CH<sub>2</sub>Cl<sub>2</sub> (25 mL), and the reaction mixture continued to stir overnight at room temperature. The red-orange reaction mixture was concentrated to dryness, and the residue was purified by flash chromatography (silica, 20% hexanes in CH<sub>2</sub>Cl<sub>2</sub>) and afforded **5** as a dark orange solid (924 mg, 44% over two steps). <sup>1</sup>H NMR (400 MHz, CDCl<sub>3</sub>): δ 2.08 (6H, s), 3.84 (3H, s), 4.67 (2H, s), 6.18 (2H, d, J = 4 Hz), 6.31 (2H, d, J = 4.4 Hz), 6.64 (2H, s). <sup>13</sup>C NMR (100 MHz, CDCl<sub>3</sub>): δ 20.3, 52.4, 65.2, 113.3, 117.2, 128.1, 128.7, 138.2, 138.6, 138.9, 141.5, 157.6, 169.5. LRESI-MS calculated for [MH<sup>+</sup>] 405.1, found 405.1.

**3,7-Dichloro-5,5-difluoro-10-(4-(2-methoxy-2-oxoethoxy)-2,6-dimethylphenyl)-5H-dipyrrolo[1,2-c:2',1'-f][1,3,2]diazaborinin-4-ium-5-uide (5)**. Distilled DIEA (1.78 mL, 10.2 mmol) was added dropwise to a solution of **4** (924 mg, 2.3 mmol) in anhydrous CH<sub>2</sub>Cl<sub>2</sub> (25 mL), and the resulting solution was allowed to stir for an additional 20 min. BF<sub>3</sub>·OEt<sub>2</sub> (2.6 mL, 20.5 mmol) was then added dropwise over a period of 5 min, and the resulting solution was allowed

to stir overnight. The reaction mixture was quenched with water (100 mL) and then extracted with CH<sub>2</sub>Cl<sub>2</sub> (3 × 25 mL). The organics were combined, dried over Na<sub>2</sub>SO<sub>4</sub>, filtered, and dried *in vacuo*. Purification by flash chromatography (silica, 10% hexanes in CH<sub>2</sub>Cl<sub>2</sub>) gave **5** as a red-orange solid with a green luster (771 mg, 75%). <sup>1</sup>H NMR (400 MHz, CDCl<sub>3</sub>): δ 2.06 (6H, s), 3.80 (3H, s), 4.65 (2H, s), 6.34 (2H, d, J = 4 Hz), 6.58 (2H, d, J = 4.4 Hz), 6.65 (2H, s). <sup>13</sup>C NMR (100 MHz, CDCl<sub>3</sub>): δ 20.2, 52.3, 64.9, 113.6, 119.0, 123.3, 130.3, 134.2, 138.5, 143.1, 144.8, 158.2, 169.1. LRESI-MS calculated for [MH<sup>+</sup>] 453.1, found 453.0.

**3-Chloro-5,5-difluoro-7-methoxy-10-(4-(2-methoxy-2-oxoethoxy)-2,6-dimethylphenyl)-5H-dipyrrolo[1,2-c:2',1'-f][1,3,2]diazaborinin-4-ium-5-uide (6)**. A solution of **5** (771 mg, 17 mmol) in anhydrous THF (40 mL) was cooled to 0 °C, and 25 wt % sodium methoxide (398 mg, 18.4 mmol) in anhydrous MeOH (90 mL) was added dropwise in two portions over 2.5 h. The reaction mixture was maintained at 0 °C for 4 h until the reaction was complete by TLC analysis. The solvent was removed *in vacuo*, and the resulting solid was partitioned between water (50 mL) and CH<sub>2</sub>Cl<sub>2</sub> (3 × 50 mL). The organics were combined, dried over Na<sub>2</sub>SO<sub>4</sub>, filtered, and dried *in vacuo*. Purification by flash chromatography (silica, CH<sub>2</sub>Cl<sub>2</sub>) delivered **6** as a red-orange solid (640 mg, 84%). <sup>1</sup>H NMR (400 MHz, CDCl<sub>3</sub>): δ 2.08 (6H, s), 3.83 (3H, s), 4.13 (3H, s), 4.65 (2H, s), 6.10 (1H, d, J = 4.8 Hz), 6.20 (1H, d, J = 4.0 Hz), 6.31 (1H, d, J = 4 Hz), 6.65 (2H, s), 6.70 (1H, d, J = 4.4 Hz). <sup>13</sup>C NMR (100 MHz, CDCl<sub>3</sub>): δ 20.3, 52.4, 59.3, 65.1, 104.9, 113.5, 115.5, 124.8, 125.2, 130.7, 132.4, 133.9, 137.0, 139.0, 139.2, 158.0, 169.3, 169.6. LRESI-MS calculated for [MH<sup>+</sup>] 449.1, found 449.1.

**3-(Bis(2-((2-(ethylthio)ethyl)thio)ethyl)amino)-5,5-difluoro-7-methoxy-10-(4-(2-methoxy-2-oxoethoxy)-2,6-dimethylphenyl)-5H-dipyrrolo[1,2-c:2',1'-f][1,3,2]diazaborinin-4-ium-5-uide (8)**. Anhydrous MeCN (10 mL) was added to **6** (185 mg, 413 μmol) and **7** (575 mg, 1.8 mmol). The reaction mixture was purged with a stream of N<sub>2</sub> for 5 min and continued to stir at 45 °C in the dark for 72 h. The reaction mixture was concentrated to dryness. Purification by column chromatography (silica, 0.5% toluene in CH<sub>2</sub>Cl<sub>2</sub> to 0.25% MeOH in CH<sub>2</sub>Cl<sub>2</sub> to 0.5% MeOH in CH<sub>2</sub>Cl<sub>2</sub>) provided **8** as a red oil (168 mg, 56%). <sup>1</sup>H NMR (400 MHz, CDCl<sub>3</sub>): δ 1.20 (6H, t, J = 7.4 Hz), 2.05 (6H, s), 2.53 (4H, q, J = 7.4 Hz), 2.70–2.74 (4H, m), 2.77–2.81 (4H, m), 2.86 (4H, t, J = 7.2 Hz), 3.79 (3H, s), 3.89 (4H, t, J = 7.4 Hz), 3.93 (3H, s), 4.62 (2H, s), 5.60 (1H, d, J = 4 Hz), 5.94 (1H, d, J = 4.8 Hz), 6.09 (1H, d, J = 3.6 Hz), 6.41 (1H, d, J = 4.8 Hz), 6.60 (2H, s). <sup>13</sup>C NMR (100 MHz, CDCl<sub>3</sub>): δ 14.8, 20.2, 25.6, 30.1, 31.8, 32.2, 52.3, 53.3, 58.0, 65.0, 94.9, 110.0, 113.1, 121.7, 125.5, 126.8, 131.5, 133.0, 139.3, 157.3, 159.7, 161.6, 169.4. LRESI-MS calculated for [MH<sup>+</sup>] 726.3, found 726.3.

**3-(Bis(2-((2-(ethylthio)ethyl)thio)ethyl)amino)-10-(4-(carboxymethoxy)-2,6-dimethylphenyl)-5,5-difluoro-7-methoxy-5H-dipyrrolo[1,2-c:2',1'-f][1,3,2]diazaborinin-4-ium-5-uide (Carboxy-CS1 9)**. Powdered LiOH (20 mg, 833 μmol) was added to a solution of **8** (168 mg, 231 μmol) in anhydrous MeOH (3 mL) and anhydrous THF (3 mL), and the reaction mixture continued to stir overnight at room temperature. The reaction mixture was concentrated *in vacuo*, dissolved in water (15 mL), and the pH was adjusted to pH 1–2 with 0.5 M HCl. The reaction mixture was extracted with CHCl<sub>3</sub> (2 × 25 mL), and the organics were combined, dried over Na<sub>2</sub>SO<sub>4</sub>, filtered, and dried *in vacuo*. Purification by column chromatography (silica, 1.5% MeOH in CH<sub>2</sub>Cl<sub>2</sub>) yielded **9** as a red oil (98 mg, 60%). <sup>1</sup>H NMR (400 MHz, CDCl<sub>3</sub>): δ 1.24 (6H, t, J = 7.2 Hz), 2.10 (6H, s), 2.57 (4H, q, J = 7.2 Hz), 2.73–2.78 (4H, m), 2.81–2.85 (4H, m), 2.89 (4H, t, J = 7.2 Hz, J = 7.6 Hz), 3.93 (4H, t, J = 7.4 Hz), 3.97 (3H, s), 4.71 (2H, s), 5.64 (1H, d, J = 4.4 Hz), 5.96 (1H, d, J = 4.8 Hz), 6.13 (1H, d, J = 4 Hz), 6.45 (1H, d, J = 4.8 Hz), 6.66 (2H, s). <sup>13</sup>C NMR (100 MHz, CDCl<sub>3</sub>): δ 14.8, 20.3, 26.0, 30.3, 31.7, 31.9, 32.2, 32.5, 53.3,

58.1, 64.7, 95.0, 110.1, 113.2, 121.8, 125.6, 127.2, 131.4, 131.6, 133.0, 139.6, 157.0, 159.8, 161.7, 173.6. LRESI-MS calculated for  $[\text{MH}^+]$  712.2, found 712.2.

**(2-Aminoethyl)triphenylphosphonium Bromide (10).** Compound **10** was prepared according to a previously reported procedure with the following modifications: the crude solid was triturated with diethyl ether as reported, but it was not further recrystallized from ethanol/diethyl ether as reported. The characterization data were consistent with results previously reported in the literature.<sup>93</sup>

**Mitochondrial Coppersensor-1 (Mito-CS1, 11).** Compound **9** (98 mg, 137  $\mu\text{mol}$ ) and HATU (59 mg, 155  $\mu\text{mol}$ ) were dissolved in anhydrous  $\text{CH}_2\text{Cl}_2$  (6 mL) and purged with a stream of  $\text{N}_2$  for 5 min. After 20 min, **10** (59 mg, 153  $\mu\text{mol}$ ) was added in one portion, and the reaction mixture continued to stir for 20 min. Distilled DIEA was added after 20 min, and the reaction was stirred at room temperature overnight. The reaction mixture was concentrated *in vacuo* and purified by column chromatography (first column: silica, 0.25% EtOAc and 0.25% MeOH in  $\text{CH}_2\text{Cl}_2$ ; second column, silica, 0.5% EtOAc and 0.5% MeOH in  $\text{CH}_2\text{Cl}_2$ ; third column, silica, 0.25% EtOAc and 0.25% MeOH in  $\text{CH}_2\text{Cl}_2$  to 1% MeOH in  $\text{CH}_2\text{Cl}_2$ ) to furnish **11** as a red semisolid (67 mg, 48%).  $^1\text{H}$  NMR (400 MHz,  $\text{CDCl}_3$ ):  $\delta$  1.23 (6H, t,  $J = 7.2$  Hz,  $J = 7.6$  Hz), 2.07 (6H, s), 2.56 (4H, q,  $J = 7.4$  Hz), 2.72–2.76 (4H, m), 2.80–2.84 (4H, m), 2.88 (4H, t,  $J = 7.4$  Hz), 3.52 (2H, p,  $J = 7.2$  Hz), 3.74 (2H, p,  $J = 6.4$  Hz,  $J = 7.2$  Hz), 3.91 (4H, t,  $J = 7.4$  Hz), 3.95 (3H, s), 4.34 (2H, s), 5.62 (1H, d,  $J = 4$  Hz), 5.95 (1H, d,  $J = 4.8$  Hz), 6.11 (1H, d, 4 Hz), 6.45 (1H, d,  $J = 4.8$  Hz), 6.71 (2H, s), 7.67–7.83 (15H, m).  $^{13}\text{C}$  NMR (100 MHz,  $\text{CDCl}_3$ ):  $\delta$  14.8, 20.2, 26.0, 30.3, 31.9, 32.4, 33.3, 53.3, 58.0, 66.6, 95.0, 110.1, 113.4, 117.1, 117.9, 121.9, 125.7, 126.9, 130.7, 130.8, 133.4, 133.5, 135.5, 139.3, 156.9, 159.7, 169.5. HRESI-MS calculated for  $[\text{M}^+]$  999.3576, found 999.3585.

**Rhodamine 123.** Rhodamine 123 was prepared according to a previously reported procedure with the following modifications: the crude solid was triturated with chloroform, and the resulting solid was collected via vacuum filtration and washed with chloroform. Characterization was consistent with that previously reported in the literature.<sup>94</sup>

**Spectroscopic Materials and Methods.** Millipore water was used to prepare all aqueous solutions. All spectroscopic measurements were performed in phosphate buffered saline (1X PBS, pH 7.4, Invitrogen, Carlsbad, CA). Absorption spectra were recorded on a Varian Cary 50 spectrophotometer (Walnut Creek, CA), and fluorescence spectra were recorded using a Photon Technology International Quanta Master 4 L-format scanning spectrofluorometer (Lawrenceville, NJ) equipped with an LPS-220B 75-W xenon lamp and power supply, A-1010B lamp housing with integrated igniter, switchable 814 photon-counting/analog multiplier detection unit, and MD5020 motor driver. Samples for absorption and emission measurements were contained in 1 cm  $\times$  1 cm path length quartz cuvettes (1.4 mL volume, Starna, Atascadero, CA). Fluorescence quantum yields were determined by reference to rhodamine 101 inner salt in methanol ( $\Phi = 1.0$ ).<sup>95</sup> The binding affinity of  $\text{Cu}^+$  to Mito-CS1 was measured using thiourea as a competitive ligand to provide a buffered  $\text{Cu}^+$  solution. Stability constants for thiourea binding were taken from the literature,  $b_{12} = 2.0 \times 10^{12}$ ,  $b_{13} = 2.0 \times 10^{14}$ ,  $b_{14} = 3.4 \times 10^{15}$ .<sup>96</sup> Thiourea was delivered from an aqueous stock solution (200 mM, 500 mM).  $\text{Cu}^+$  was delivered in the form of  $[\text{Cu}(\text{MeCN})_4[\text{PF}_6]]$  from an acetonitrile stock solution (1 mM, 5 mM). Excitation was provided at 540 nm, and collected emission was integrated from 550 to 700 nm after 1 or 2 min after the addition of dye or metal analyte. The apparent dissociation constant ( $K_d$ ) was determined using the following equation:  $(F - F_{\text{min}})/(F_{\text{max}} - F_{\text{min}}) = [\text{Cu}^+]/(K_d + [\text{Cu}^+])$ , where  $F$  is the observed fluorescence,  $F_{\text{max}}$  is the fluorescence for the  $\text{Cu}^+$ :Mito-CS1 complex,  $F_{\text{min}}$  is the fluorescence for free Mito-CS1, and  $[\text{Cu}^+]$  is the “free”  $\text{Cu}^+$  available for complexation, which was calculated using the stability constants for thiourea and standard competition equilibrium expressions. All other metal ions

tested for metal ion selectivity studies with the exception of  $\text{Fe}^{2+}$  were from their chloride salts as aqueous solutions. Ammonium iron(II) sulfate hexahydrate was used as a source of  $\text{Fe}^{2+}$ , and the salt was dissolved in degassed water.

**Preparation of Cell Cultures.** Cells were grown in the Tissue Culture Facility at the University of California, Berkeley, with expert technical assistance from Ann Fischer and Michelle Yasukawa. HEK 293T cells were cultured in Dulbecco's Modified Eagle Medium (DMEM, Invitrogen, Carlsbad, CA) containing high glucose and without phenol red supplemented with GlutaMAX (Invitrogen, Carlsbad, CA) and 10% Fetal Bovine Serum (FBS, Hyclone, Logan, UT). Two days before imaging, cells were passed and plated on 12 mm glass coverslips coated with poly-L-lysine (50 mg/mL, Sigma, St. Louis, MO). Control, *ATP7A*, *SCO1*, and *SCO2* fibroblasts were cultured in Dulbecco's Modified Eagle Medium (DMEM, Invitrogen, Carlsbad, CA) containing high glucose and without phenol red supplemented with GlutaMAX (Invitrogen, Carlsbad, CA), 1 mM sodium pyruvate, and 10% Fetal Bovine Serum (FBS, Hyclone, Logan, UT). Two days before imaging, cells were passed and plated on 12 mm glass coverslips or 4-well chambered coverglass slides.

**Cell Staining.** For all experiments, solutions of Mito-CS1 (from 1 or 5 mM stocks in DMSO), CS3 (from 1 mM stocks in DMSO), Rhodamine 123 (from 50  $\mu\text{M}$  stocks in DMSO), MitoTracker Deep Red (from 50  $\mu\text{M}$  stocks in DMSO), BODIPY FL C5-ceramide-BSA complex (from 1 mM stocks in water), and Hoechst 33342 (from a 5 mM stock in DMSO) were made in Dulbecco's Phosphate Buffered Saline with calcium chloride and magnesium chloride (DPBS, Invitrogen, Carlsbad, CA) or Dulbecco's Modified Eagle Medium without phenol red (DMEM, Invitrogen, Carlsbad, CA). For colocalization experiments, control HEK 293T cells were incubated with 500 nM Mito-CS1, 2.25  $\mu\text{M}$  BODIPY FL C5-ceramide-BSA complex, 50 nM Mitotracker Deep Red, and 5  $\mu\text{M}$  Hoechst 33342 for 15 min at 37  $^\circ\text{C}$ , 5%  $\text{CO}_2$  in DPBS. Coverslips were then transferred to fresh DPBS for imaging. A similar procedure was followed for imaging with 500 nM LysoTracker Green DND-26. For copper and BCS treatments, 300  $\mu\text{M}$   $\text{CuCl}_2$  or 100  $\mu\text{M}$  BCS was added to the cells from a 0.1 mM aqueous stock solution 1 day prior to imaging. Cells were then incubated at 37  $^\circ\text{C}$ , 5%  $\text{CO}_2$ . After 18 h, the media was exchanged for DPBS with 500 nM Mito-CS1 or 100 nM Rhodamine 123 and Hoechst 33342 and incubated for 15 min at 37  $^\circ\text{C}$ , 5%  $\text{CO}_2$ . Coverslips were then transferred to fresh DPBS for imaging. For colocalization experiments, control fibroblasts were incubated with 5  $\mu\text{M}$  Mito-CS1, 2.25  $\mu\text{M}$  BODIPY FL C5-ceramide-BSA complex, and 5  $\mu\text{M}$  Hoechst 33342 for 15 min at 37  $^\circ\text{C}$ , 5%  $\text{CO}_2$  in DPBS. A similar procedure was followed for imaging with 250 nM LysoTracker Green DND-26 in DMEM. Coverslips were then transferred to fresh DPBS for imaging. MitoTracker Deep Red (50 nM in DPBS) was added on stage and then imaged. For BCS treatment, 100  $\mu\text{M}$  BCS was added to the cells from a 0.1 mM aqueous stock solution 1 day prior to imaging. After 12 h, the media was exchanged for DMEM with 5  $\mu\text{M}$  Mito-CS1 or 100 nM Rhodamine 123 and 5  $\mu\text{M}$  Hoechst 3342 and incubated for 15 min at 37  $^\circ\text{C}$ , 5%  $\text{CO}_2$ . Coverslips were then transferred to fresh DPBS for imaging. Similar procedures were followed for imaging changes in mitochondrial  $\text{Cu}^+$  in the wild-type, *ATP7A*, *SCO1*, and *SCO2* fibroblasts. For copper treatment, 300 or 500  $\mu\text{M}$   $\text{CuCl}_2$  was added to the cells from a 0.1 mM aqueous stock solution 1 day prior to imaging. After 18 h, the medium in the chambered coverglass slides was exchanged for DMEM with 5  $\mu\text{M}$  Mito-CS1 or 100 nM Rhodamine 123 and 5  $\mu\text{M}$  Hoechst 3342 and incubated for 15 min at 37  $^\circ\text{C}$ , 5%  $\text{CO}_2$ , washed with fresh DPBS, and imaged in fresh DPBS. Control and *ATP7A* patient fibroblasts were stained with 2  $\mu\text{M}$  CS3 and incubated for 10 min at 37  $^\circ\text{C}$ , 5%  $\text{CO}_2$  in DPBS, washed with fresh DPBS, and imaged in fresh DPBS.

**Fluorescence Imaging Experiments.** Confocal fluorescence images were acquired at the Molecular Imaging Center at the University



of California, Berkeley. Imaging experiments were performed with a Zeiss LSM510 META NLO Axioplan 2 laser-scanning microscope, a Zeiss 510NL META AxioIMAGER laser-scanning microscope, and a Zeiss LSM 710 laser-scanning microscope with a 40× or 63× water-immersion objective lens. Excitation of Mito-CS1 or CS3 loaded cells at 543 nm was carried out with a HeNe laser, and emission was collected using a META detector between 554 and 650 nm. Excitation of LysoTracker Green DND-26 at 488 nm was carried out with an Ar laser, and emission was collected using a META detector between 501 and 533 nm. Excitation of BODIPY FL C5-ceramide-BSA complex at 488 nm was carried out with an Ar laser, and emission was collected using a META detector between 498 and 511 nm. Excitation of Rhodamine 123 at 488 nm was carried out with an Ar laser, and emission was collected using a META detector between 501 and 576 nm. Excitation of MitoTracker Deep Red at 633 nm was carried out with a HeNe laser, and emission was collected using a META detector between 640 and 704 nm. Excitation of Hoechst 33342 was carried out using a MaiTai two photon laser at 780 nm pulses or a 405 nm diode laser, and emission was collected between 469 and 522 nm with Rhodamine 123 and 447 and 533 nm for all other dyes. ImageJ from the National Institutes of Health was used for analysis of the images. Specifically, the threshold for a field of cells was adjusted to select the pixels and was kept consistent in a given experiment. The selected pixels were analyzed for the median value. The mean of the median value for *n* fields of cells with standard error is reported, and statistical analyses were performed with a two-tailed Student's *t*-test in Microsoft Excel.

**ICP-OES Analysis**<sup>36</sup>. Mitochondria and whole cells were digested in 40% nitric acid by boiling for 1 h in capped, acid-washed tubes; samples were then diluted in ultrapure, metal-free water, and analyzed by ICP-OES (PerkinElmer, Optima 3100XL). Acid-washed blanks were used as controls. Concentrations were determined from a standard curve constructed with serial dilutions of commercially available mixed metal standards (Optima). Error bars cannot be added to the data points for mitochondria isolated from *SCO1* and *SCO2* patient liver, due to the scarcity of the material; the total tissue sample only consists of milligram quantities originating from a metabolic autopsy, thus precluding additional, large-scale analyses. Furthermore, we did not have access to liver samples from deceased *ATP7A* patients. To minimize any potential effects associated with experimental variability, mitochondria were isolated on the same day using identical buffers and reagents from each patient sample. Each sample was then split into two aliquots, and total mitochondrial copper content was quantified in duplicate by ICP-OES in the same run.

**Miscellaneous Procedures.** COX and citrate synthase activities were measured in HEK 293T and fibroblast cell extracts as described elsewhere.<sup>32,97</sup> Protein concentration was measured by the Bradford method.<sup>98</sup>

## ■ ASSOCIATED CONTENT

Supporting Information. Additional imaging and biochemical data and full reference information. This material is available free of charge via the Internet at <http://pubs.acs.org>.

## ■ AUTHOR INFORMATION

**Corresponding Author**  
chrischang@berkeley.edu

## ■ ACKNOWLEDGMENT

We thank the Packard Foundation (C.J.C.), the Hellman Faculty Fund (C.J.C.), Amgen (C.J.C.), Astra Zeneca (C.J.C.), Novartis (C.J.C.), and the National Institute of General Medical Sciences

(NIH GM 79465 to C.J.C., NIH GM 083292 to D.R.W.) for funding this work. C.J.C. is an Investigator with the Howard Hughes Medical Institute. We thank Holly Aaron (UCB Molecular Imaging Center) and Ann Fischer and Michelle Yasukawa (UCB Tissue Culture Facility) for expert technical assistance and helpful discussions.

## ■ REFERENCES

- (1) Gray, H. B.; Stiefel, E. I.; Valentine, J. S.; Bertini, I. *Biological Inorganic Chemistry: Structure and Reactivity*, 1st ed.; University Science Books: California, 2006.
- (2) Turski, M. L.; Thiele, D. J. *J. Biol. Chem.* **2009**, *284*, 717–721.
- (3) Banci, L.; Bertini, I.; Ciofi-Baffoni, S.; Kozyreva, T.; Zovo, K.; Paulmaa, P. *Nature* **2010**, *465*, 645–648.
- (4) Camakaris, J.; Voskoboinik, I.; Mercer, J. F. *Biochem. Biophys. Res. Commun.* **1999**, *261*, 225–232.
- (5) Rosenzweig, A. C.; O'Halloran, T. V. *Curr. Opin. Chem. Biol.* **2000**, *4*, 140–147.
- (6) O'Halloran, T. V.; Culotta, V. C. *J. Biol. Chem.* **2000**, *275*, 25057–25060.
- (7) Lee, J.; Marjorette, M. O.; Nose, Y.; Thiele, D. J. *J. Biol. Chem.* **2002**, *277*, 4380–4387.
- (8) Rees, E. M.; Lee, J.; Thiele, D. J. *J. Biol. Chem.* **2004**, *279*, 54221–54229.
- (9) Fontaine, S. L.; Mercer, J. F. *Arch. Biochem. Biophys.* **2007**, *463*, 149–167.
- (10) Davis, A. V.; O'Halloran, T. V. *Nat. Chem. Biol.* **2008**, *4*, 148–151.
- (11) Kim, B.-E.; Nevitt, T.; Thiele, D. J. *Nat. Chem. Biol.* **2008**, *4*, 176–185.
- (12) Prohaska, J. R. *Am. J. Clin. Nutr.* **2008**, *88*, 826S–829S.
- (13) Kaplan, J. H.; Lutsenko, S. *J. Biol. Chem.* **2009**, *284*, 25461–25465.
- (14) Ma, Z.; Jacobsen, F. E.; Giedroc, D. P. *Chem. Rev.* **2009**, *109*, 4644–4681.
- (15) Boal, A. K.; Rosenweig, A. C. *Chem. Rev.* **2009**, *109*, 4760–4779.
- (16) Hass, K. L.; Franz, K. J. *Chem. Rev.* **2009**, *109*, 4921–4960.
- (17) White, C.; Lee, J.; Kambe, T.; Fritsche, K.; Petris, M. J. *J. Biol. Chem.* **2009**, *284*, 33949–33956.
- (18) Barry, A. N.; Shinde, U.; Lutsenko, S. *J. Biol. Inorg. Chem.* **2010**, *15*, 47–59.
- (19) McRae, R.; Lai, B.; Fahrni, C. J. *J. Biol. Inorg. Chem.* **2010**, *15*, 99–105.
- (20) Bertini, I.; Cavallaro, G.; McGreevy, K. S. *Coord. Chem. Rev.* **2010**, *254*, 506–524.
- (21) Banci, L.; Bertini, I.; McGreevy, K. S.; Rosato, A. *Nat. Prod. Rep.* **2010**, *27*, 695–710.
- (22) Robinson, N. J.; Winge, D. R. *Annu. Rev. Biochem.* **2010**, *79*, 537–562.
- (23) Banci, L.; Bertini, I.; Cantini, F.; Ciofi-Baffoni, S. *Cell. Mol. Life Sci.* **2010**, *67*, 2563–2589.
- (24) Rubino, J. T.; Riggs-Gelasco, P.; Franz, K. J. *J. Biol. Inorg. Chem.* **2010**, *15*, 1033–1049.
- (25) Cobine, P. A.; Pierrel, F.; Winge, D. R. *Biochim. Biophys. Acta* **2006**, *1763*, 759–772.
- (26) Pierrel, F.; Cobine, P. A.; Winge, D. R. *Biomaterials* **2007**, *20*, 675–682.
- (27) Horn, D.; Barrientos, A. *IUBMB Life* **2008**, *60*, 421–429.
- (28) Abriata, L. A.; Banci, L.; Bertini, I.; Ciofi-Baffoni, S.; Gkazonis, P.; Spyroulias, G. A.; Vila, A. J.; Wang, S. *Nat. Chem. Biol.* **2008**, *4*, 599–601.
- (29) Leary, S. C.; Winge, D. R.; Cobine, P. A. *Biochim. Biophys. Acta* **2009**, *1793*, 146–153.
- (30) Atkinson, A.; Winge, D. R. *Chem. Rev.* **2009**, *109*, 4708–4721.
- (31) Cobine, P. A.; Pierrel, F.; Bestwick, M. L.; Winge, D. R. *J. Biol. Chem.* **2006**, *281*, 36552–36559.

- (32) Leary, S. C.; Kaufman, B. A.; Pellicchia, G.; Guercin, G.; Mattman, A.; Jaksch, M.; Shoubridge, E. A. *Hum. Mol. Genet.* **2004**, *13*, 1839–1848.
- (33) Williams, J. C.; Sue, C.; Banting, G. S.; Yang, H.; Glerum, D. M.; Hendrickson, W. A.; Schon, E. A. *J. Biol. Chem.* **2005**, *280*, 15202–15211.
- (34) Horng, Y. C.; Leary, S. C.; Cobine, P. A.; Young, F. B. J.; George, G. N.; Shoubridge, E. A.; Winge, D. R. *J. Biol. Chem.* **2005**, *280*, 34113–34122.
- (35) Matoba, S.; Kang, J. G.; Patino, W. D.; Wragg, A.; Boehm, M.; Gavrilova, O.; Hurley, P. J.; Bunz, F.; Hwang, P. M. *Science* **2006**, *312*, 1650–1653.
- (36) Leary, S. C.; Cobine, P. A.; Kaufman, B. A.; Guercin, G.; Mattman, A.; Palaty, J.; Lockitch, G.; Winge, D. R.; Rustin, P.; Horvath, R.; Shoubridge, E. A. *Cell Metab.* **2007**, *5*, 9–20.
- (37) Banci, L.; Bertini, I.; Cavallaro, G.; Rosato, A. *J. Proteome Res.* **2007**, *6*, 1568–1579.
- (38) Banci, L.; Bertini, I.; Ciofi-Baffoni, S.; Hadjiloi, T.; Martinelli, M.; Palumaa, P. *Proc. Natl. Acad. Sci. U.S.A.* **2008**, *105*, 6803–6808.
- (39) Rigby, K.; Cobine, P. A.; Khalimonchuk, O.; Winge, D. R. *J. Biol. Chem.* **2008**, *283*, 15015–15022.
- (40) Leary, S. C.; Sasarman, F.; Nishimura, T.; Shoubridge, E. A. *Hum. Mol. Genet.* **2009**, *18*, 2230–2240.
- (41) Sung, H. J.; Ma, W.; Wang, P.; Hynes, J.; O’Riordan, T. C.; Combs, C. A.; McCoy, J. P., Jr.; Bunz, F.; Kang, J. G.; Hwang, P. M. *Nat. Commun.* **2010**, *1*, 1–8.
- (42) Stiburek, L.; Zeman, J. *Biochim. Biophys. Acta* **2010**, *1797*, 1149–1158.
- (43) Leary, S. C. *Antioxid. Redox Signaling* **2010**, *13*, 1403–1416.
- (44) Banci, L.; Bertini, I.; Ciofi-Baffoni, S.; Kozyreva, T.; Mori, M.; Wang, S. *J. Biol. Inorg. Chem.* **2011**, *16*, 391–403.
- (45) Papadopoulou, L. C.; Sue, C. M.; Davidson, M. M.; Tanji, K.; Nishino, I.; Sadlock, J. E.; Krishna, S.; Walker, W.; Selby, J.; Glerum, D. M.; *Nat. Genet.* **1999**, *23*, 333–337.
- (46) Jaksch, M.; Ogilvie, I.; Yao, J.; Hortenhaus, G.; Bresser, H. G.; Gerbitz, K. D.; Shoubridge, E. A. *Hum. Mol. Genet.* **2000**, *9*, 795–801.
- (47) Horvath, R.; Lochmüller, Stucka, R.; Yao, J.; Shoubridge, E. A.; Kim, S. H.; Gerbitz, K. D.; Jaksch, M. *Biochem. Biophys. Res. Commun.* **2000**, *276*, 530–533.
- (48) Valnot, I.; Osmond, S.; Gigarel, N.; Mehaye, B.; Amiel, J.; Corneir-Daire, V.; Munnich, A.; Bonnefont, J. P.; Rustin, P.; Rotig, A. *Am. J. Hum. Genet.* **2000**, *67*, 1104–1109.
- (49) Jaksch, M.; Horvath, R.; Horn, N.; Auer, D. P.; Macmillan, C.; Peters, J.; Gerbitz, K. D.; Kraegeloh-Mann, I.; Muntau, A.; Karcagi, V.; Kalmanchev, R.; Lochmüller, H.; Shoubridge, E. A.; Freisinger, P. *Neurology* **2001**, *57*, 1440–1446.
- (50) Jaksch, M.; Paret, C.; Stucka, R.; Horn, N.; Müller-Höcker, J.; Horvath, R.; Trepesch, N.; Stecker, G.; Fresinger, P.; Thirion, C.; Müller, J.; Lunckwitz, R.; Rödel, G.; Shoubridge, E. A.; Lochmüller, H. *Hum. Mol. Genet.* **2001**, *10*, 3025–3035.
- (51) Salvati, L.; Hernandez-Rosa, E.; Walker, W. F.; Sacconi, S.; Dimauro, S.; Schon, E. A.; Davidson, M. M. *Biochem. J.* **2002**, *363*, 321–327.
- (52) Hamza, I.; Giltin, J. D. *J. Bioenerg. Biomembr.* **2002**, *34*, 381–388.
- (53) Foltopoulou, P. F.; Zachariadis, G. A.; Politou, A. S.; Tsiftoglou, A. S.; Papadopoulou, L. C. *Mol. Genet. Metab.* **2004**, *81*, 225–236.
- (54) Stiburek, L.; Vesela, K.; Hansikova, H.; Pecina, P.; Tesarova, M.; Cerna, L.; Houstek, J.; Zeman, J. *Biochem. J.* **2005**, *392*, 625–632.
- (55) Cobine, P. A.; Pierrel, F.; Leary, S. C.; Sasarman, F.; Horng, Y.; Shoubridge, E. A.; Winge, D. R. *J. Biol. Chem.* **2006**, *281*, 12270–12276.
- (56) Leary, S. C.; Mattman, A.; Wai, T.; Koehn, D. C.; Clarke, L. A.; Chan, S.; Lomax, B.; Eydoux, P.; Vallance, H. D.; Shoubridge, E. A. *Mol. Genet. Metab.* **2006**, *89*, 129–133.
- (57) Banci, L.; Bertini, I.; Ciofi-Baffoni, S.; Leontari, I.; Martinelli, M.; Palumaa, P.; Sillard, R.; Wang, S. *Proc. Natl. Acad. Sci. U.S.A.* **2007**, *104*, 15–20.
- (58) Stiburek, L.; Vesela, K.; Hansikova, H.; Hulkova, H.; Zeman, J. *Am. J. Physiol. Cell Physiol.* **2009**, *296*, C1218–C1226.
- (59) Yang, H.; Broesel, S.; Acin-Perez, R.; Slavkovich, V.; Nishino, I.; Khan, R.; Goldberg, I. J.; Graziano, J.; Manfredi, G.; Schon, E. A. *Hum. Mol. Genet.* **2010**, *19*, 170–180.
- (60) Zeng, L.; Miller, E. W.; Pralle, A.; Isacoff, E. Y.; Chang, C. J. *J. Am. Chem. Soc.* **2006**, *128*, 10–11.
- (61) Miller, E. W.; Zeng, L.; Domaille, D. W.; Chang, C. J. *Nat. Protoc.* **2006**, *1*, 824–827.
- (62) Que, E. L.; Chang, C. J. *J. Am. Chem. Soc.* **2006**, *128*, 15942–15943.
- (63) Domaille, D. W.; Que, E. L.; Chang, C. J. *Nat. Chem. Biol.* **2008**, *4*, 168–175.
- (64) Que, E. L.; Domaille, D. W.; Chang, C. J. *Chem. Rev.* **2008**, *108*, 1517–1549.
- (65) Que, E. L.; Chang, C. J. *Chem. Soc. Rev.* **2010**, *39*, 51–60.
- (66) Que, E. L.; Gianolio, E.; Barker, S. L.; Aime, S.; Chang, C. J. *Dalton Trans.* **2010**, *39*, 469–476.
- (67) Domaille, D. W.; Zeng, L.; Chang, C. J. *J. Am. Chem. Soc.* **2010**, *132*, 1194–1195.
- (68) Dodani, S. C.; Domaille, D. W.; Nam, C. I.; Miller, E. W.; Finney, L. A.; Vogt, S.; Chang, C. J. *Proc. Natl. Acad. Sci. U.S.A.* **2011**, *108*, 5980–5985.
- (69) Yang, L.; McRae, R.; Henary, M. M.; Patel, R.; Lai, B.; Vogt, S.; Fahrni, C. J. *Proc. Natl. Acad. Sci. U.S.A.* **2005**, *102*, 11179–11184.
- (70) Wegner, S. V.; Arslan, H.; Sunbul, M.; Yin, J.; He, C. *J. Am. Chem. Soc.* **2010**, *132*, 2567–2569.
- (71) Taki, M.; Iyoshi, S.; Ojida, A.; Hamachi, I.; Yamamoto, Y. *J. Am. Chem. Soc.* **2010**, *132*, 5938–5939.
- (72) Merchant, S. S.; Allen, M. D.; Kropat, J.; Moseley, J. L.; Long, J. C.; Tottey, S.; Terauchi, A. M. *Biochim. Biophys. Acta* **2006**, *1763*, 578–594.
- (73) Robinson, K. M.; Janes, M. S.; Pehar, M.; Monette, J. S.; Ross, M. F.; Hagen, T. M.; Murphy, M. P.; Beckman, J. S. *Proc. Natl. Acad. Sci. U.S.A.* **2006**, *103*, 15038–15043.
- (74) Murphy, M. P.; Smith, R. A. *J. Annu. Rev. Pharmacol. Toxicol.* **2007**, *47*, 629–656.
- (75) Ross, M. F.; Prime, T. A.; Abakumova, I.; James, A. M.; Porteous, C. M.; Smith, R. A. J.; Murphy, M. P. *Biochem. J.* **2008**, *411*, 633–645.
- (76) Porteous, C. M.; Logan, A.; Evans, C.; Ledgerwood, E. C.; Menon, D. K.; Aigbirio, F.; Smith, R. A. J.; Murphy, M. P. *Biochim. Biophys. Acta* **2010**, *1800*, 1009–1017.
- (77) Dickinson, B. C.; Chang, C. J. *J. Am. Chem. Soc.* **2008**, *130*, 9638–9639.
- (78) Dickinson, B. C.; Srikun, D.; Chang, C. J. *Curr. Opin. Chem. Biol.* **2010**, *14*, 50–56.
- (79) Hardy, M.; Chalier, F.; Ouari, O.; Finet, J.; Rockenbauer, A.; Kalyanaraman, B.; Tordo, P. *Chem. Commun.* **2007**, 1083–1085.
- (80) Hoyer, A. T.; Davoren, J. E.; Wipf, M. P.; Kagan, V. E. *Acc. Chem. Res.* **2008**, *41*, 87–97.
- (81) Biasutto, L.; Matarei, A.; Marotta, E.; Bradaschia, A.; Sassi, N.; Garbisa, S.; Zoratti, M.; Paradisi, C. *Bioorg. Med. Chem. Lett.* **2008**, *18*, 5594–5597.
- (82) Ripke, J.; Zarse, K.; Ristow, M.; Birringer, M. *ChemBioChem* **2009**, *10*, 1689–1696.
- (83) Abu-Gosh, S. E.; Kolvazon, N.; Tirosh, B.; Ringel, I.; Yavin, E. *Mol. Pharmaceutics* **2009**, *6*, 1138–1144.
- (84) Yousif, L. F.; Stewart, K. M.; Kelley, S. O. *ChemBioChem* **2009**, *10*, 1939–1950.
- (85) Loudet, A.; Burgess, K. *Chem. Rev.* **2007**, *107*, 4891–4932.
- (86) Ulrich, G.; Ziesel, R.; Harriman, A. *Angew. Chem., Int. Ed.* **2008**, *47*, 1184–1201.
- (87) Hamza, I.; Prohaska, J.; Gitlin, J. D. *Proc. Natl. Acad. Sci. U.S.A.* **2003**, *100*, 1215–1220.
- (88) Chen, L. B. *Annu. Rev. Cell Biol.* **1988**, *4*, 155–81.
- (89) Johnson, L. V.; Walsh, M. L.; Chen, L. B. *Proc. Natl. Acad. Sci. U.S.A.* **1980**, *77*, 990–994.
- (90) Bellingham, S. A.; Lahiri, D. K.; Maloney, B.; Fontaine, S. L.; Multhaup, G.; Camakaris, J. *J. Biol. Chem.* **2004**, *279*, 20378–20386.

- (91) Kaler, S. G. *Nat. Rev. Neurol.* **2011**, *7*, 15–29.
- (92) Yamada, K.; Toyota, T.; Takakura, K.; Ishimaru, M.; Sugawara, T. *New J. Chem.* **2001**, *25*, 667–669.
- (93) Maryanoff, B. E.; Reitz, A. B.; Duhl-Emswiler, B. A. *J. Am. Chem. Soc.* **1985**, *107*, 217–226.
- (94) Ross, J. A.; Ross, B. P.; Rubinsztein-Dunlop, H.; McGeary, R. P. *Synth. Commun.* **2006**, *36*, 1745–1750.
- (95) Karstens, T.; Kobs, K. *J. Phys. Chem.* **1980**, *84*, 1871–1872.
- (96) Martell, A. E.; Smith, R. M. *Critical Stability Constants*; Plenum Press: New York, 1989.
- (97) Capaldi, R. A.; Marusich, M. F.; Taanman, J. W. *Methods Enzymol.* **1995**, *260*, 117–132.
- (98) Bradford, M. M. *Anal. Biochem.* **1976**, *72*, 248–254.